Lidar Measurement of Turbulence Encountered by Horizontal-Axis Wind Turbines

R. M. HARDESTY

NOAA/ERL/Wave Propagation Laboratory, Boulder, CO 80303

B. F. WEBER

Cooperative Institute for Research in the Environmental Sciences (CIRES) University of Colorado/NOAA, Boulder, CO 80309

(Manuscript received 24 February 1986, in final form 12 September 1986)

ABSTRACT

We used a continuous-wave (CW) Doppler lidar to measure wind velocity turbulence from a moving frame of reference. By directing the lidar beam to trace the perimeters of vertical-plane disks about horizontal axes parallel to the mean wind direction, we observed turbulence properties similar to those encountered by the tips of revolving turbine blades. As in other measurements made with in situ sensors, turbulence spectra observed from the moving reference points showed a decrease in energy, relative to fixed point observations, at frequencies just below the rotation frequency of the lidar beam, and an increase in energy within discrete spectral bands at higher frequencies. Comparisons with a simple model showed reasonable agreement, although measurement conditions did not correspond to the assumptions of the model. On the basis of the results of this experiment, we conclude that Doppler lidar, with appropriate signal processing, is quite applicable for measurement of turbulence encountered by spinning wind turbines.

1. Introduction

The use of horizontal-axis wind turbines to generate electrical energy has found increasing application since the early 1970s when petroleum shortages and the accompanying sharp rise in energy prices stimulated efforts to develop technology for alternative energy sources. To optimize the design of large, horizontal-axis wind turbines, mathematical models are typically employed. Typical models estimate dynamic loading on the blades and support structure, blade fatigue, power output, and control system response. A key input to such models is a realistic representation of the turbulence characteristics of the wind field encountered by the spinning turbine blade. The need for realistic wind field characterization is especially important as turbines are made increasingly larger to take advantage of economies of scale. With turbine diameters of recent prototypes approaching 70 m (Linscott et al., 1984), the blade tip moves rapidly through turbulent eddies whose energy spectra vary with environmental conditions.

The problem of measuring the wind speed at a moving point, such as the tip of a rotating turbine blade, is not easily addressed by in situ sensors. Verholek (1978) constructed a vertical-plane array of eight elevated anemometers spaced evenly around a 24-m diameter circle. The measured wind from each anemometer was recorded sequentially to obtain the desired rotationally sampled wind field. Similar measurements were later performed with the diameter of the array increased to 49 m (Connell, 1980). Although both experiments yielded good data, the difficulties involved in changing either the size of the array or its pointing angle, in combination with the potential contamination of the measured wind field by the support structures, suggest the need for a remote technique that more easily measures the turbulent properties of the wind field.

Coherent laser radar (lidar) is a well-established method for remote measurement of wind speeds in the clear air. The radial component of the wind velocity is obtained by irradiating a volume of atmosphere with optical radiation of high spectral purity and estimating the Doppler frequency shift of the radiation backscattered by small, windborne aerosol particles. In comparisons with winds measured by stationary anemometers, lidar-measured winds have been shown to correlate well and exhibit similar temporal and ensemble characteristics (Lawrence et al., 1972). Doppler systems operating in continuous-wave (CW) mode have been employed in several wind-measuring applications, including waterspout studies (Schwiesow et al., 1981) and vertical wind profiling (Kopp et al., 1984).

The primary advantage of coherent lidar for measuring the winds along the trajectory of a moving turbine blade is the relative ease in moving the point of measurement and changing the parameters describing the desired path. With a lidar, the point of measurement is moved by changing the azimuth and elevation of the lidar beam and varying the range to the scattering volume. This is typically an uncomplicated procedure:

azimuth and elevation can be easily adjusted with an appropriate scanning mechanism, while range to the measurement volume is chosen by focusing the beam, in the CW case, or time-gating the return from a pulsed system. Such procedures are usually less complicated and faster than the alternative of physically moving and setting up an array of in situ sensors, as in Verholek's (1978) method.

Although the relative ease of directing the optical beam makes lidar an attractive sensor for measuring winds at moving points in space, lidar wind measurements also have disadvantages. Since Doppler lidars measure only radial velocities, the wind measured by such systems is often a component of the wind velocity, rather than the actual wind speed. In addition, for CW lidars employing typical telescopes, range resolution is poor at ranges beyond a few hundred meters. Thus, in many cases the lidar measures velocity over volumes that are extended in range, producing a spatial filtering effect on the turbulence spectrum for small-scale turbulent features.

In this paper, the results of an experiment to measure rotationally sampled wind velocity spectra using a CW Doppler lidar are reported. The primary objective of the work was to evaluate the capabilities of the lidar technique for this application, and in the process, to provide measurement data for comparison with recently developed models that attempt to predict rotationally sampled wind turbulence. Measurements were obtained simulating several existing turbines under differing atmospheric conditions. For comparison, wind measurements from fixed anemometers mounted on an adjacent meteorological tower were sampled concurrently. Fluctuation spectra computed from the wind measurements for both cases are presented in sec. 5 and compared with results from previous measurements and simulations.

2. Background

In wind turbine design, the wind loading at particular sections of the turbine is closely related to the power spectrum of the turbulent kinetic energy. Originally, analytical techniques to calculate the load on a moving rotor used turbulence power spectra measured in a fixed frame of reference (Frost et al., 1978). However, since a typical turbine blade sweeps rapidly through regions of turbulence with dimensions as large as 122 m, the Lagrangian turbulence spectrum encountered by the moving blade tip is in general quite different from the Eulerian spectrum observed at a fixed point. Also, because wind shear in the first 100 m above the surface is often significant, a vertical-plane turbine blade may be subjected to periodic loading as it moves within the shear region.

Verholek's (1978) vertical-plane anemometer array provided the first experimental measurement of a rotationally sampled wind spectrum. The rotational spectrum showed considerable loss of energy relative to a fixed-point spectrum in the spectral decade just below the frequency of rotation of the equivalent turbine blade. In addition, the spectrum contained sharp spikes at harmonics of the rotation frequency. Verholek concluded from these results that an apparent effect of rotational sampling was to transfer the energy from intermediate to high frequencies, and to collect a large portion of this energy into narrow bands. Similar effects were later reported (Connell, 1981) in measurements from both a larger anemometer array and a hot-wire anemometer mounted on a rotating 3.8-m-radius boom.

In efforts to explain these observations, Connell (1981) and Kristensen and Frandsen (1982) developed models independently that gave results showing good qualitative agreement with the observation of Verholek. Assuming homogeneity and isotropy in the wind field, and applying Taylor's hypothesis, Kristensen and Frandsen compute the normalized autocovariance function of the rotationally sampled wind as

$$\rho(s)=\frac{2}{\Gamma(1/3)}(\alpha^2\sin^2 s+\beta^2 s^2)^{1/6}\times\left\{K_{1/3}[2(\alpha^2\sin^2 s+\beta^2 s^2)^{1/2}]-\frac{\alpha^2\sin^2 s}{(\alpha^2\sin^2 s+\beta^2 s^2)^{1/2}}K_{2/3}[2(\alpha^2\sin^2 s+\beta^2 s^2)^{1/2}]\right\}, \quad (1)$$

where

$$\alpha = a/L,$$

$$\beta = \frac{\langle u_1\rangle}{L\omega_0},$$

$$s = \omega_0\tau/2,$$

and a is the radius of the circular motion of the turbine blade tip, L a velocity length scale characterizing the turbulence, $\langle u_1\rangle$ the mean longitudinal wind velocity, ω_0 the frequency of rotation of the turbine, Γ the gamma function, τ time and $K_{1/3}$ and $K_{2/3}$ are modified Bessel functions of the second kind of orders 1/3 and 2/3, respectively.

Kristenson and Frandsen (1982) compared results from this model with a spectrum of the measured wind load on the vane of the Gedser wind turbine in Denmark. The model results showed good agreement with the observed results up to the second harmonic of the rotation frequency; the authors declined to discuss the spectrum at frequencies greater than the second harmonic because of uncertainty regarding the effects of the turbine structure on the measured load.

Because of the difficulty involved in changing the parameters of in situ measurements, we have investigated the use of lidar techniques to obtain additional experimental data for comparison with the models. A preliminary experiment using a simple CW laser system

to measure the rotational spectra sampled around a small (10 m diameter) circle, although limited by low system sensitivity, indicated promise for the technique (Hardesty et al., 1981a). The present work was aimed at extending the previous results by examining in greater detail the rotational spectra for several turbine configurations ranging in diameter from 38 to 122 m. Such an effort emphasizes the potential advantage of using lidar to obtain the measurements. Because varying the scan parameters is relatively easy with the lidar technique, it was possible to make measurements simulating several turbines within a fairly short period of time.

3. Equipment description

Figure 1 shows the configuration employed to measure rotationally sampled winds. The beam from the trailer-mounted National Oceanic and Atmospheric Administration (NOAA) lidar was directed by the system scanner onto a second scanner mounted on the movable carriage of the 300-m high Boulder Atmospheric Observatory (BAO) tower (Kaimal and Gaynor, 1983). This carriage-mounted scanner consisted of a rotating shaft with a 30-cm diameter mirror mounted at the end. The mirror was mounted with its centerline axis skewed relative to the shaft axis, so that the mirror nutated as the motor shaft was rotated. Through appropriate choice of the shaft angle and mirror angle, the incident lidar beam was made to trace out a horizontal-axis cone during a rotation of the shaft. Rotation rate of the shaft, corresponding to the rotation rate of the virtual wind turbine, was controlled by a dc motor.

The NOAA lidar, which has been described in previous works (e.g., Hardesty et al., 1983), was parked adjacent to the tower system as depicted in Fig. 1. Throughout the experiment the lidar was operated in CW mode to improve on the minimum-range and range-resolution limitations that exist when the transmitter is pulsed. Because in CW mode the laser transmitter produced approximately 1 W of coherent output power, the minimum backscatter coefficient for usable velocity measurements was on the order of 10^{-9} m^{-1} sr^{-1}. Table 1 lists the principal operating parameters for the system operating in CW mode. The CW power was provided by a low-pressure gain cell within the laser transmit cavity. To reduce cavity losses, the flow chamber of the intracavity transverse excited atmospheric (TEA) laser used to provide the energy during pulsed operation was evacuated to below 0.01 atm pressure.

When the lidar is operated in CW mode, scattering volume dimensions and range selection are functions of the distance to the lidar beam focus. The transverse radius of the scattering volume at the focus is approximated by (Dickson, 1969)

$$r_s \approx \frac{2\lambda z_f}{\pi D}, \tag{2}$$

where z_f is the distance to the focus, λ wavelength, and D the diameter of the optical telescope. Normally, transverse scattering volume radius is less than 1 cm for typical system parameters; this is orders of magnitude smaller than the volume radial dimension. Near the beam focus, the range weighting function $F(z)$ of

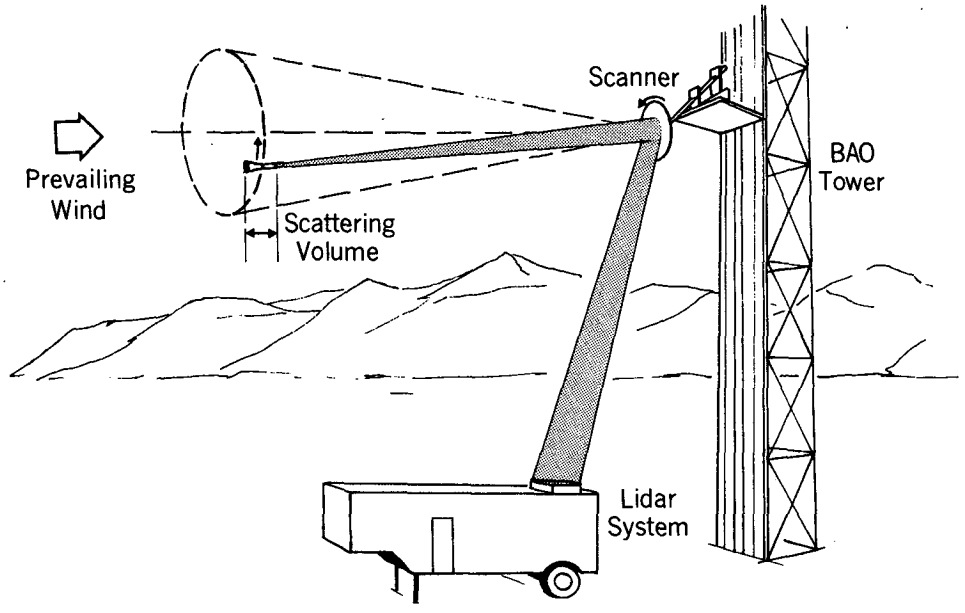

FIG. 1. Schematic diagram of the geometry for lidar measurement of rotationally sampled winds, using the BAO tower to support the scanning mirror. The cone angle was maintained at 10° for all measurements; radius of the base of the measurement cone was varied by beam focusing.

TABLE 1. Operating parameters for lidar wind turbine experiments.

Parameter	Value
Lidar	
Mode	Continuous wave
Wavelength (μm)	10.6
Output power (W)	1
Aperture diameter (m)	0.28
Signal Processing	
Spectral estimation technique	Frequency-swept spectrum analyzer
Velocity resolution (m s^{-1})	0.16
Measurement rate (Hz)	5–10
Minimum measurable wind speed (m s^{-1})	1.5

the system is inversely proportional to the beam area (Dickson); i.e.,

$$F(z) = \frac{K\pi^2 D^2}{4\lambda^2 z^2\left[1 + \frac{\pi^2 D^4}{16\lambda^2}(1/z - 1/z_f)^2\right]} \quad (3)$$

where K is a constant of proportionality, and it is assumed that the e^{-2} diameter of the output beam is matched to the telescope diameter. From Eq. (3) the radial dimension of the scattering volume (defined in this case as the region over which $F(z)$ is greater than or equal to one-half its value at the focus) can be estimated. Figure 2 shows estimates of both the radial length and transverse diameter of the scattering volume calculated from Eqs. (2) and (3) for the NOAA lidar as a function of the distance to the beam focus. It is seen that both dimensions increase with range; however the width of the scattering volume is approximately three orders of magnitude less than its length. Also shown in Fig. 2 is the estimated range-weighting function for the NOAA lidar focused at distances of 427, 322, and 147 m, corresponding to the turbine measurement cases of interest. As the distance to the focus increases, range resolution decreases significantly.

Doppler processing of the lidar returns was carried out with a conventional frequency-swept spectrum analyzer, from which an estimate of the Doppler spectrum was digitized and stored on magnetic tape. The 30-kHz resolution intermediate frequency (IF) filter (equivalent to a velocity resolution of 0.16 m s^{-1}), was swept across the 2 MHz receiver bandwidth in 10 ms. The dwell time of the swept filter within a given frequency interval was about twice the filter time constant, hence on the order of two independent samples of the power within each resolution element were obtained during a single spectrum analyzer sweep. Although a spectrum was obtainable every 10 ms, digitizer and data transfer constraints limited the actual spectrum storage rate to one per 100 ms, which was the desired velocity sampling rate. Since only a single spectrum was used to form the velocity estimate, speckle-induced random power fluctuations within each spectrum element represented a major source of measurement noise. The radial wind estimate was computed off-line from the digitized spectrum by measuring the Doppler shift of the spectral peak. Because of the optical feedthrough effects in the lidar system, winds could not be measured when the radial wind speed was below about 1.5 m s^{-1}. This minimum velocity constraint was not a major limitation, since turbulence tends to affect wind turbines more when winds are strong. The amount of energy in the peak of the Doppler spectrum was used to estimate signal quality; measurements with marginal signal strength were rejected.

4. Properties of the lidar-measured wind estimates

Ideally, the rotationally sampled wind measurements obtained by the lidar would be identical to the longitudinal wind sampled at a point moving on the radius of a horizontal-axis circle. In reality, lidar measurements deviate from the ideal in several ways. The most important differences are the following:

1) *Lidar measures the radial wind component only.* When winds are rotationally sampled using the conical scan configuration shown in Fig. 1, the pointing vector of the lidar beam is slightly offset from the horizontal wind vector, which ideally is aligned with the axis of the scanned cone. Thus, as the lidar beam is scanned around the base of the cone, harmonics of the rotation frequency are introduced into the longitudinal wind measurement due to the projection onto the lidar pointing vector of the wind components transverse to the cone axis (i.e., the crosswind and vertical components). These components can become more significant as the cone angle is increased. Similarly, since the direction of the cone axis ideally remains fixed throughout a measurement case, temporal variations in wind direction also cause changes in the magnitude of the projection of the horizontal wind vector onto the lidar pointing vector.

2) *The lidar signal is composed of returns from relatively long volumes.* During CW operation, each irradiated scatterer within the scattering volume produces a signal whose frequency is Doppler-shifted according to the particle's radial velocity. Thus, the mean (average of many realizations) power spectrum is equivalent to a histogram of average radial velocity within the entire scattering volume, with each spectral component weighted by the intensity of the total return from scatterers moving at the corresponding velocity. From this spectrum, it is generally not possible to determine exactly the wind velocity at a single point within the volume.

3) *The instantaneous aerosol-backscattered lidar signal spectrum is a random process.* The instantaneous signal within a given frequency increment at the receiver is the vector sum of the signals backscattered by those individual aerosol particles within the scattering volume that are moving at the appropriate radial ve-

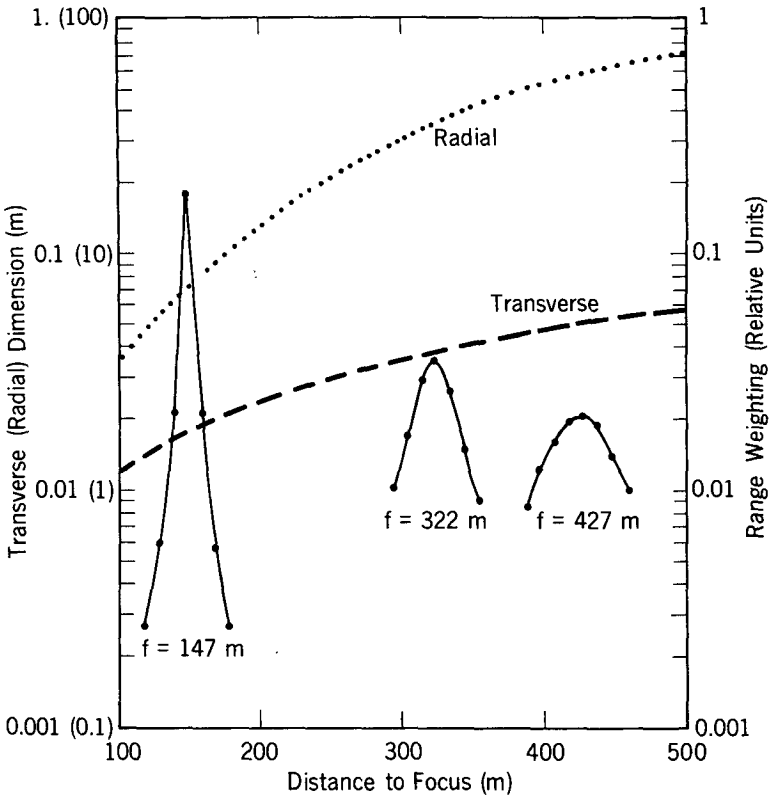

FIG. 2. Approximate transverse diameter (dashed line) and radial length (dotted line) of the scattering volume for the NOAA lidar, as calculated from Eqs. (2) and (3), vs range. Also shown are range weighting functions (solid lines) for the lidar beam when focused at ranges of 427, 322 and 147 m, corresponding to the measurement cases of interest.

locities. Since the phases of the individual signals are random, the resultant signal is a random process whose amplitude and phase characteristics vary over time as the relative positions of the particles change because of the small-scale velocity turbulence; this is the well-known problem of laser speckle (see, e.g., Hardesty et al., 1981b). Instantaneously, the backscattered power within a given spectral increment can be modeled as an exponentially distributed random process, whose mean is roughly proportional to the number of particles with Doppler-shifted frequencies that lie within the frequency increment. Consequently, the instantaneous signal spectrum is not representative of the intensity-weighted histogram of velocities within the scattering volume; some method of spectral averaging is necessary to obtain a reasonable estimate of mean velocity distribution.

The foregoing properties must be taken into account when selecting and interpreting results of algorithms to estimate wind velocity from the backscattered-signal spectrum. Most Doppler processing schemes compute velocity from either the mean frequency of the Doppler spectrum or the frequency corresponding to the peak spectral energy. Since observations of Doppler spectra obtained during the experiment showed that the spectra were generally symmetric and unimodal, both methods would have produced estimates with similar expected values. We chose to use a spectral peak estimator for this analysis, primarily because it was slightly easier to implement than an estimator based on the spectral mean.

The performance of a frequency estimator for atmospheric returns based on the spectral peak has been examined in a related work (Hardesty, 1986). When the intensity-weighted density function of radial velocities in the scattering volume is Gaussian and the bandwidth of a filter element is much narrower than the signal bandwidth, a peak estimate based on a single spectral realization at high signal-to-noise ratio (SNR) has a standard deviation that is approximately 0.6 times the spectral width of the wind velocity probability density function. As SNR decreases, the standard deviation of the estimate gets larger, since the probability increases that a frequency increment containing only noise will have the highest instantaneous power and be selected as the velocity estimate.

5. Measurement results

A series of rotationally sampled wind measurements was obtained during June and July of 1983. Scanner geometry and lidar system parameters were chosen to simulate wind loading on three existing wind turbines, the characteristics of which are described in Table 2 (the 122-m diameter turbine was studied at three different rotation rates). The BAO instrument carriage supporting the scanner was raised or lowered as required, to change the equivalent hub height of the simulated turbine. Rotation rate of the simulated turbine was adjusted by varying the rotation rate of the dc motor that spun the shaft of the optical scanner assembly.

To simulate the two larger turbines described in Table 2, the diameter of the base of the cone scanned by the lidar had to be made relatively large. We had a choice of two techniques to increase the circle radius, both of which produced undesirable effects on the measurement. As seen from Eq. (3), holding the cone angle constant and increasing the distance to the lidar focus increases the radial dimension of the scattering volume, making the lidar measurement less representative of the desired point measurement. The alternative technique, maintaining a constant focus and increasing the cone angle, yields a measurement averaged over a smaller radial distance; however, the measured radial wind is less representative of the longitudinal wind. Because we wanted to minimize the total measurement time in order to reduce the probability of a significant wind shift during the measurements, we chose to keep the cone angle constant throughout the experiment and vary only the focal distance to change the simulated turbine radius (focal distance could be adjusted much more easily than cone angle). The distance to the lidar focus and the radial length of the scattering volume for each of the five turbine cases are also listed in Table 2.

At the start of a measurement, the tower anemometer wind measurement from the level closest to the tower-mounted scanner height was used to set the cone axis of the lidar scan parallel to the prevailing wind direction. After a run commenced, the lidar azimuth angle was not changed unless the wind direction shifted enough that the radial component measured by the lidar was less than the minimum detectable velocity. When possible, data relating to each turbine were collected for at least 20 min in order to characterize the low-frequency components of the wind fluctuation spectrum. Because high-frequency spectral characteristics are also important in examining the effects of rotational sampling, the lidar wind measurements were sampled at a minimum of ten times the scanner rotation rate. Concurrent with the lidar measurements, tower instrumentation recorded in situ measurements of horizontal and vertical wind speeds, temperature, stability, and other relevent parameters at each of the eight instrumentation levels.

Ideally, we had hoped to collect data during periods when the wind speed was greater than about 4 m s^{-1} with relatively constant direction for periods of 2 h or more, so as to compare under similar atmospheric conditions the turbulence spectra relating to different turbines. Unfortunately, these conditions rarely were present during the experiment period, primarily because of the climatological conditions that exist during the summer months near the Front Range of the Rocky Mountains. During most summer days, light winds in the early morning are followed by an onset of valley flow by midday. The winds during this period of valley flow are often fairly steady until early or midafternoon, when small-scale outflows from convective cells frequently perturb the background flow. Initially, we attempted to obtain a complete measurement set during the interval between the onset of the valley flow and the disruption of the large-scale wind pattern by the convective outflow. This turned out to be exceedingly difficult. Although one or two 20-min measurement sets were generally obtainable, not once in seven attempts was the wind sufficiently steady for a complete set of five measurements to be completed.

The lack of success with daytime measurements prompted an attempt to find a potentially acceptable measurement period during the night. Examination of records from BAO archives showed that drainage flows from the mountains 30 km west of the BAO, which typically arrived at the site after sunset, often were characterized by intervals during which wind field properties were acceptable. Three sets of nighttime measurements were taken beginning approximately 2 h after sunset. These intervals produced better results than the daytime measurements; winds on two of the

TABLE 2. Turbine characteristics (Linscott et al., 1984) and lidar focusing parameters for cases studied.

Case	Turbine	Hub height (m)	Diameter (m)	Rotation speed (rpm)	Distance to lidar focus (m)	Approximate radial length of scattering volume (m)
1	Mod-5A	76.2	122	10	427	64
2	Mod-5A	76.2	122	15	427	64
3	Mod-5A	76.2	122	20	427	64
4	Mod-2	61.0	91.5	17.5	322	36
5	Mod-0A	30.5	38.1	40	147	7

three nights were sufficiently consistent for us to complete 20-min wind measurement segments for all five of the simulated turbines listed in Table 2.

One measurement set chosen for detailed analysis was taken on the night of 1–2 July 1983. Figure 3 shows 20-min time series of lidar and tower-measured winds for three of the five cases listed in Table 2, corresponding to three different-sized turbines. Each point plotted represents a 10-s average (equivalent to approximately two to six revolutions around the scanned circle) of lidar-measured wind speeds. Tower measurements shown in the figure were formed from the projection onto the cone axis of the lidar scan of the wind vector measured by the tower anemometer closest in height to the cone axis.

As in similar studies by Lawrence et al. (1972), the lidar and tower measurements agree quite well, especially considering the spatial separation and size differences between the two measurement volumes. An apparent slight phase difference between the lidar and tower time series seen in case 5 is probably due to a start-time discrepancy of about 1 min in the two data sets. Table 3 shows mean ($\bar{u}_T$), standard deviation (σ_{u_T}), and correlation coefficient ($\rho_{u_L u_T}$) values calcu-

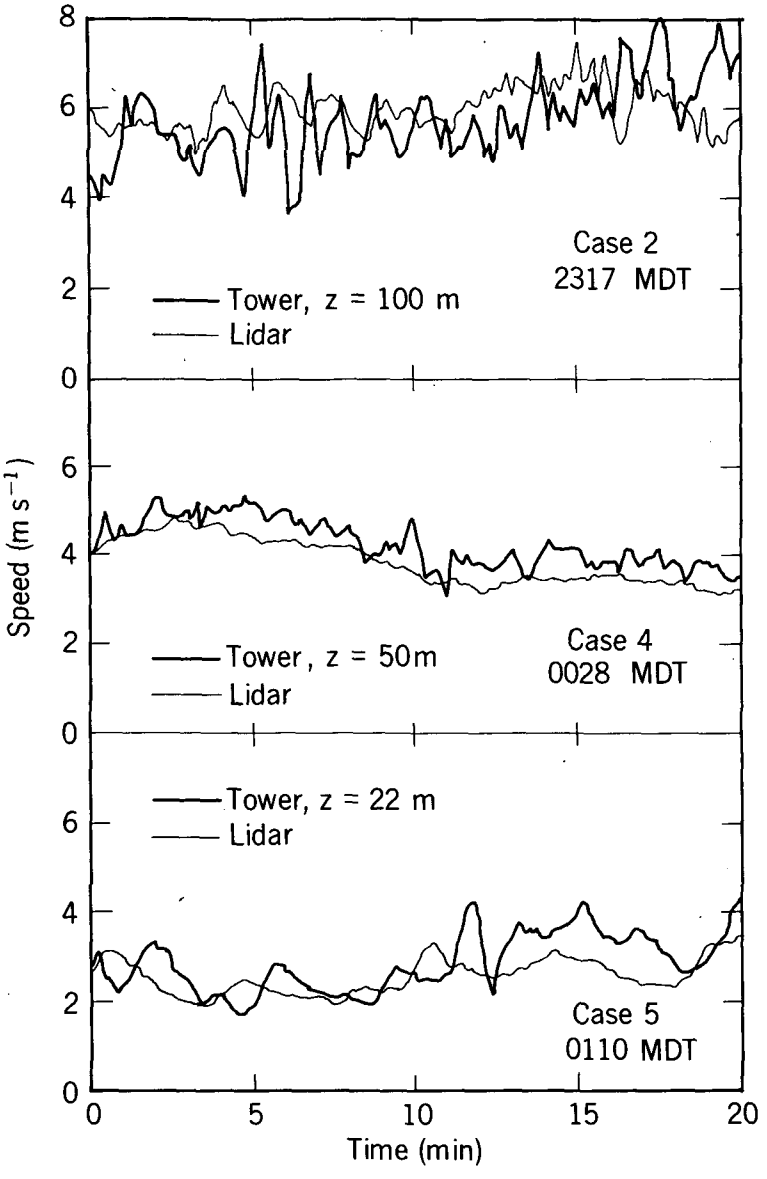

FIG. 3. Time series of 10-s averaged wind speeds measured by lidar and by the nearest anemeometers on the tower for three turbine cases, taken 1–2 July 1983, showing good agreement between the sensors. Anemometer measurements are resolved along the lidar pointing vector for each case. Cases refer to designations in Table 2.

TABLE 3. Comparison of lidar and tower sonic anemometer wind measurement statistics, computed from 10-s averaged data, for 1–2 July 1983 measurements. (Tower measurements are projected along the lidar pointing vector.)

Parameter	Case 2 2317 MDT	Case 4 0028 MDT	Case 5 0110 MDT
Tower			
Anemometer height (m)	100	50	22
$\bar{u}_T$ (m s^{-1})	5.78	4.29	2.90
σ_{u_T} (m s^{-1})	0.96	0.53	0.65
Lidar			
Scanner (cone axis) height (m)	76	61	30
Pointing azimuth (deg)	300	240	210
$\bar{u}_L$ (m s^{-1})	5.95	3.88	2.60
σ_{u_L} (m s^{-1})	0.48	0.51	0.41
Correlation coefficient			
$\rho_{u_L u_T}$	0.06	0.86	0.49

lated for the different 10-s averaged wind measurements. Mean values for the tower and lidar were within 0.5 m s^{-1} for each of the three cases; the lidar measurements exhibited smaller standard deviations, especially in the case 2 comparison. In this case the tower measurements were characterized by considerable short-term fluctuations, which increased the measurement standard deviation and reduced the correlation coefficient. Note in Table 3 how the cone axis of the lidar scan had to be changed for each case in order to keep the axis pointing into the mean wind.

The 10 s average on the data of Fig. 3 removes the evidence of rotational wind field sampling from the lidar time series. Rotational sampling effects are obvious in Fig. 4, which shows 30 s segments of concurrent lidar and tower wind measurements for each of the three cases. In contrast to the tower measurements, the lidar-measured winds exhibit very strong periodicities at the scanner rotation frequency. Amplitude of the periodic fluctuations is a function of the diameter of the circle circumscribed by the lidar beam. Cases 2 and 4, corresponding to larger turbine diameters, exhibit higher amplitude fluctuations than case 5. Since the amplitudes of the fluctuations are proportional to differences between extremes of the horizontal wind measured by the lidar on a single revolution, one expects the cases that scan around larger diameter circles to exhibit greater variability, because of both the increased shear across the larger circles and the effect of moving the measurement point through turbulent eddies of larger size and amplitude. Average wind shears measured by the tower were approximately 2.5 m s^{-1} over the vertical region scanned by the lidar in case 2, 1.5 m s^{-1} over the region scanned in case 4, and 0.5 m s^{-1} over the case 5 region, which are in rough agreement with the observed fluctuations in Fig. 4. The measurements from the tower anemometers show that short-term variability of the Eulerian-sampled wind speeds (i.e., speeds measured at a fixed point) was much less than that of those sampled in the moving frame of reference.

From the time series of wind speeds illustrated in Figs. 3 and 4, we computed fluctuation spectra for both the tower and lidar measurements, as shown in Fig. 5. In the figure, tower and lidar spectra are smoothed logarithmically with smoothing windows of 0.1 and 0.025 times the center frequency, respectively. (The width of the lidar data smoothing window was made narrower so as not to broaden the sharp spectral peaks artifically.) It is seen that the effects observed by Verholek (1978), i.e., strong spectral components at harmonics of the rotation frequency combined with decreases in spectral energy in the low-frequency portion of the rotationally sampled wind spectra relative to the in situ cases, are also present in the lidar-measured wind spectra. Measurement noise, resulting from the frequency measurement uncertainties discussed in section 4, is obvious in the high-frequency portions of the lidar spectra for cases 4 and 5, where the +1 slope in the power spectrum indicating white noise is evident. Although this noise obscures all but the peaks in the wind turbulence spectra at frequencies above about 0.2 Hz, it does not prevent observation of the spectral energy decrease at the lower frequencies due to rotational sampling. Note that this relative loss of low-frequency energy is most evident in cases 2 and 4, in which the Eulerian spectra more closely approximate a classic $f^{-5/3}$ power law ($f^{-2/3}$ in this representation), and is less obvious for the case closest to the ground (case 5). These results are consistent with observations by Connell (1981) that the effects of rotational sampling increase with the ratio a/L, where a is the radius of the scanned circle circle and L is the turbulence length scale. In case 5, a is one-third that of case 2; in addition, the Eulerian spectrum from case 5 shows a drop in energy at frequencies above 0.02 Hz, indicative of a larger value for L. Hence, the greater effect of rotational sampling for case 2 is not surprising. Because case 2 also appears to have the least noise contamination at high frequencies, as well as a Eulerian spectrum approximating a classical Kolmogorov spectrum, it best illustrates the effects of rotationally sampling a classical Kolmogorov wind field.

In Fig. 6 the lidar-measured spectra of rotationally sampled winds are compared with spectra predicted by the model of Eq. (1) for each of the three cases analyzed. Because of data transfer constraints, we computed the model spectra over 1024 points, which produced some sidelobe contamination, as can be observed in the spectra. Acoustic sounder records of turbulence structure were used to estimate scale size of the velocity fluctuations in each case for input to the model. The comparisons show at least a qualitative agreement with the model results for the various cases; the agreement is quite good for case 2 and poorest for case 5. Both the model predictions and measurement

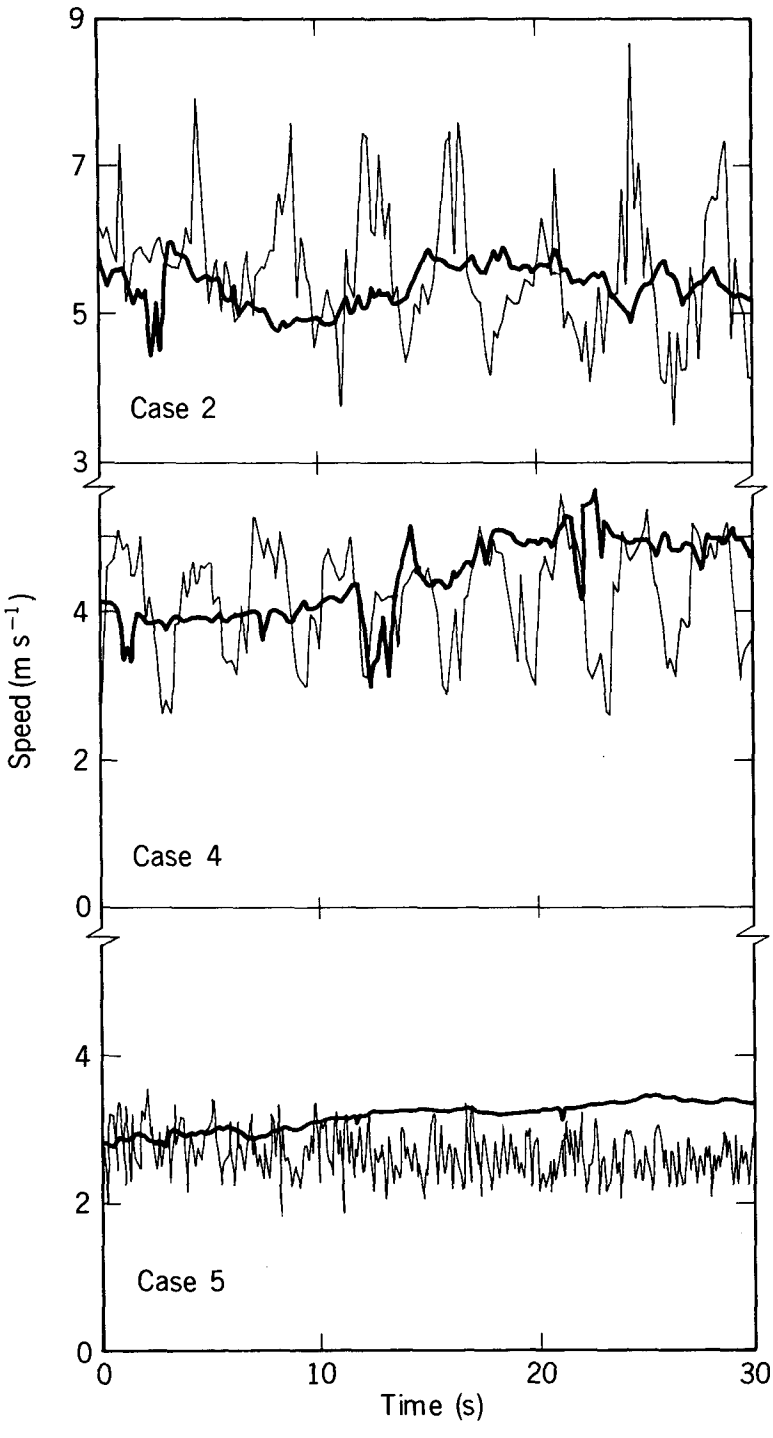

FIG. 4. Short (30 s) segments of lidar (fine lines) and tower (bold lines) wind speed measurements for three turbine cases of 1–2 July 1983, showing periodic components in lidar data resulting from rotational sampling. Tower measurements are resolved along the lidar pointing direction. All tower measurements were sampled at 10 Hz; lidar measurements were sampled at 5 Hz for cases 2 and 4, and 10 Hz for case 5.

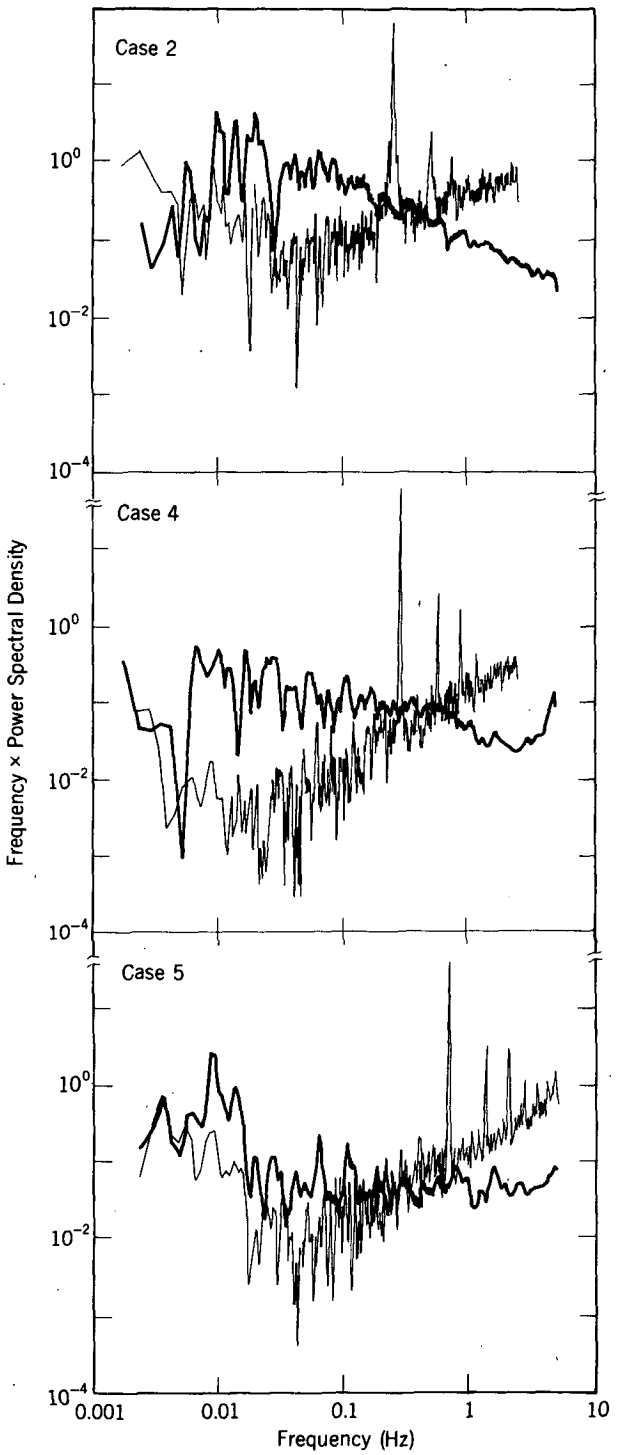

FIG. 5. Fluctuation spectra of lidar (fine lines) and tower (bold lines) winds computed from 1–2 July 1983 measurements, showing a low-frequency spectral energy decrease and harmonic components in the lidar-measured spectra as a result of rotational sampling. Each spectrum was calculated after removing the mean and applying a triangular window to the data sequence.

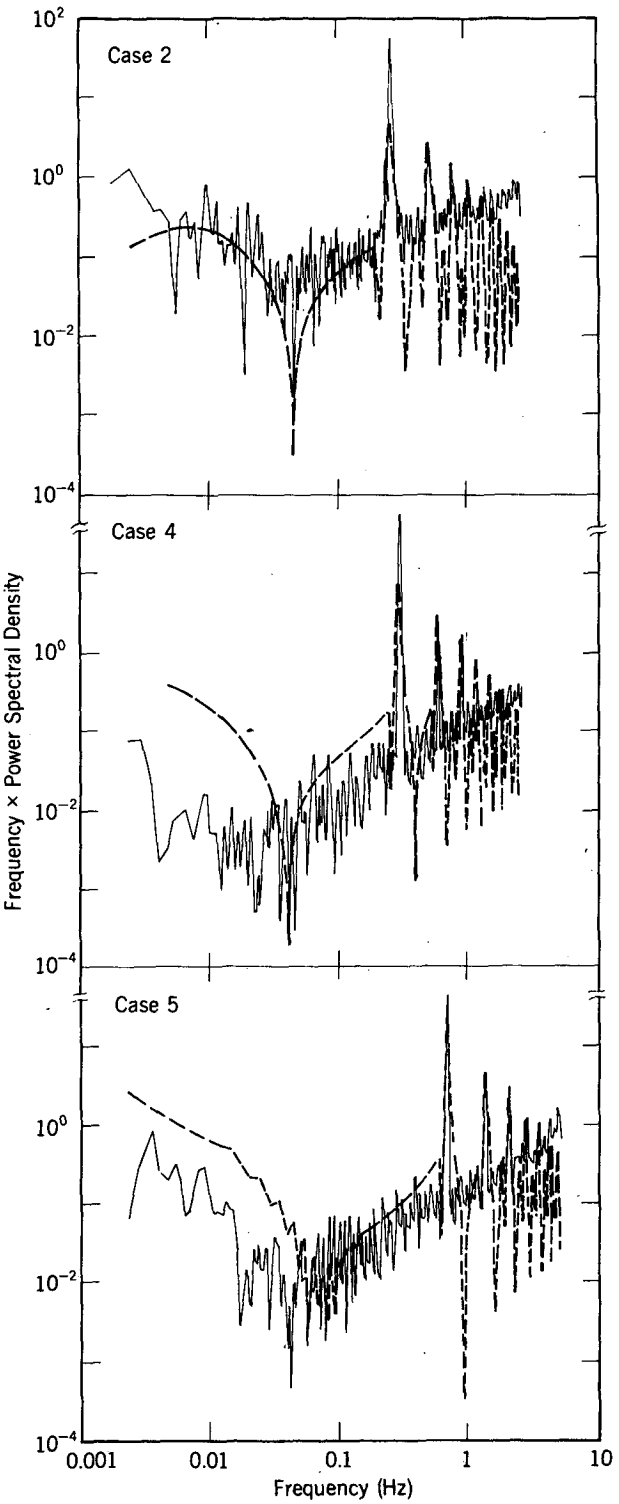

FIG. 6. Fluctuation spectra of lidar (fine lines) as in Fig. 5, compared with predicted spectra (dashed lines) computed from Eq. (1) for 1–2 July 1983 cases. Evidence of sidelobes in the model spectra is due to the short (1024-point) data sequence.

results show a broadening of the spectral peaks as the diameter of the turbine increases. However, the peaks in the lidar spectra are somewhat narrower than either those predicted by the model, or observed by Kristenson and Frandsen (1982) in their measurements of the spectra of fluctuation in the stay force on a large turbine. This could indicate that vertical shear, rather than turbulence, contributed a significant portion of the energy to the spectral peaks, since rotational sampling of a static nonlinear vertical shear profile produces a spectrum composed of harmonics of the rotation frequency. Mean wind profiles measured by the tower-mounted anemometers showed that nonlinear shear was present during each of the measurement periods.

It can be seen in Figs. 5 and 6 that energy in the higher order harmonics of the rotation frequency (i.e., beyond the third harmonic) is somewhat suppressed, especially for cases 2 and 4. One potential explanation for this lack of energy in the higher harmonics observed in the lidar spectra is the effect of spatial averaging resulting from the relatively long lidar resolution volumes. Assuming that the estimate of wind velocity obtained from the processing algorithm is roughly equivalent to the mean wind over the volume, the long lidar resolution volume has the effect of applying a low-pass filter over the spatial distribution of velocities. We can estimate this effect on the spectra plotted in Figs. 5 and 6 by approximating Eq. (3) with a Gaussian-shaped resolution volume and calculating the approximate equivalent filter response from

$$H(f) = \exp\left[\frac{-f^2}{2(\bar{u}/\sigma_r)^2}\right], \tag{4}$$

where $\bar{u}$ is the mean longitudinal wind, σ_r the standard deviation of the Gaussian radial weighting function, and f frequency. Figure 7 shows the estimated filter response functions plotted in the spectral domain as computed for the three cases examined in Figs. 3–6. Note the sharp falloff in response at the higher frequencies due to the long volumes. Figure 7 indicates that attenuation of higher frequencies as a result of spatial filtering should be greater for cases 2 and 4 than case 5; the results plotted in Figs. 5 and 6 do show significantly more high frequency energy in the case 5 spectra. The presence of fifth, sixth and seventh harmonics in the case 5 spectrum is somewhat surprising, however, since the filtering effect should attenuate these frequencies. Evidence of these harmonics tends to support the observation that some of the energy in the spectrum, especially at these frequencies, results from rotational sampling of a static nonlinear vertical profile, rather than from sampling of the turbulence field.

When comparing the spectra measured by the lidar in Fig. 6 with those predicted by Eq. (1), it is important to note the meteorological conditions that prevailed during the measurement. On the night of 1–2 July, synoptic maps showed two fronts bracketing Colorado: one extended across central Wyoming and the other was in western Kansas. The strong pressure gradient produced the relatively brisk winds observed during the measurements. Examination of acoustic sounder and tower sensor records also showed evidence of boundary layer waves during the period. Figure 8 shows a time series of temperature measured at the eight different tower heights for a 20-min period beginning at 2300 MDT, just prior to the start of case 2. The lack of stationarity, as indicated by the presence of a sharp discontinuity midway through the data, is typical of the other segments. As further evidence of atmospheric variability, measurements of Monin-Obukhov length indicated that stability near the surface fluctuated markedly during the experiment. The lower boundary layer was predominantly unstable during cases 2 and 5, and stable during case 4. Under such variable conditions, assumptions of homogeniety and stationarity, made in the development of the model used for the comparisons shown in Fig. 6, are almost certainly not valid. Consequently, the apparent agreement between the observed and model spectra is probably somewhat fortuitous, although similar qualitative agreement was reported by Kristensen and Frandsen (1982) in their comparisons using the Gedser turbine. This would seem to indicate that strict stationarity and homogeneity are not always necessary conditions for the model to produce realistic spectral estimates.

6. Summary and concluding remarks

This experiment, though hampered by undesirable weather conditions throughout the data collection period, demonstrates that CW Doppler lidar is a viable technique for measuring wind velocities from a moving frame of reference. The advantage of lidar techniques over in situ measurements, such as those employed by Verholek (1978), lies in the relative ease of altering the measurement parameters. Within a period of about 2 h, we were able to examine turbulence properties over measurement geometries corresponding to five different turbine cases. Comparable measurements would be almost impossible to make with an elevated array of in situ sensors because of the difficulty involved in changing the measurement geometry.

When compared with spectra computed from the fixed-point tower anemometer wind measurements, rotationally sampled lidar turbulence spectra showed properties similar to those observed in previous works, i.e., a decrease in energy in the spectral region just below the rotational frequency, an increase in energy in the high-frequency portion of the spectrum, and a bunching of energy at frequencies around the harmonics of the rotational frequency. Despite the fact that the atmospheric conditions were generally more complex than those assumed in derivation of a simple model, the measurement results also agreed qualitatively with those predicted by the model. However, because the data set was limited by the uncooperative atmospheric conditions, additional data taken under more ideal cir-

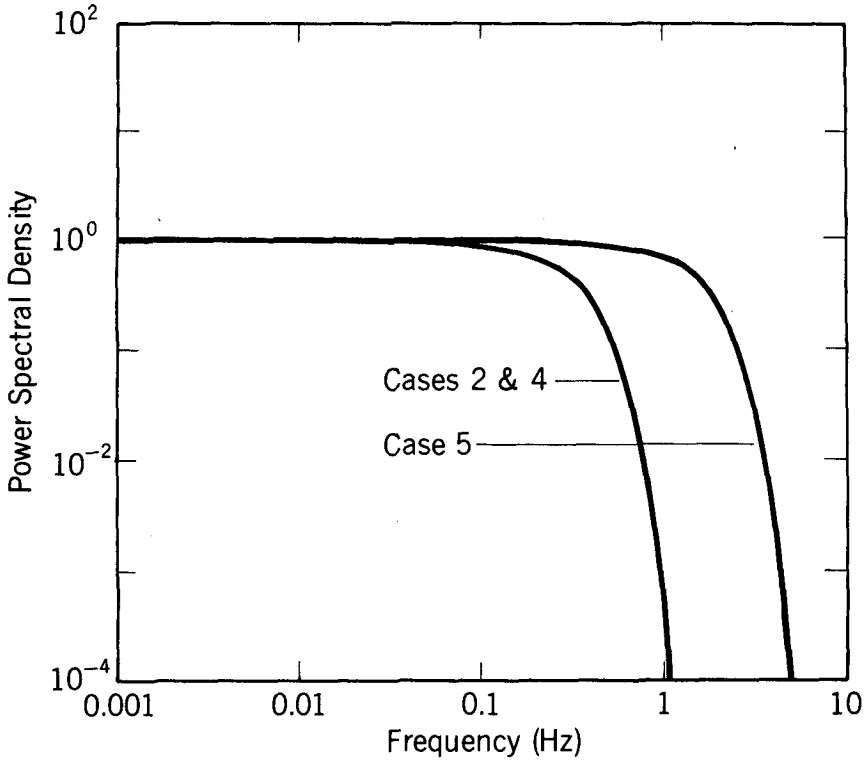

FIG. 7. Estimated response of the spatial filter caused by long lidar resolution volume, for the three measurement cases of 1–2 July 1983. The nearly identical responses of cases 2 and 4 is largely coincidental; the decrease in measurement volume size for case 4 was almost exactly compensated for by a decrease in longitudinal wind speed, resulting in the same filter effect.

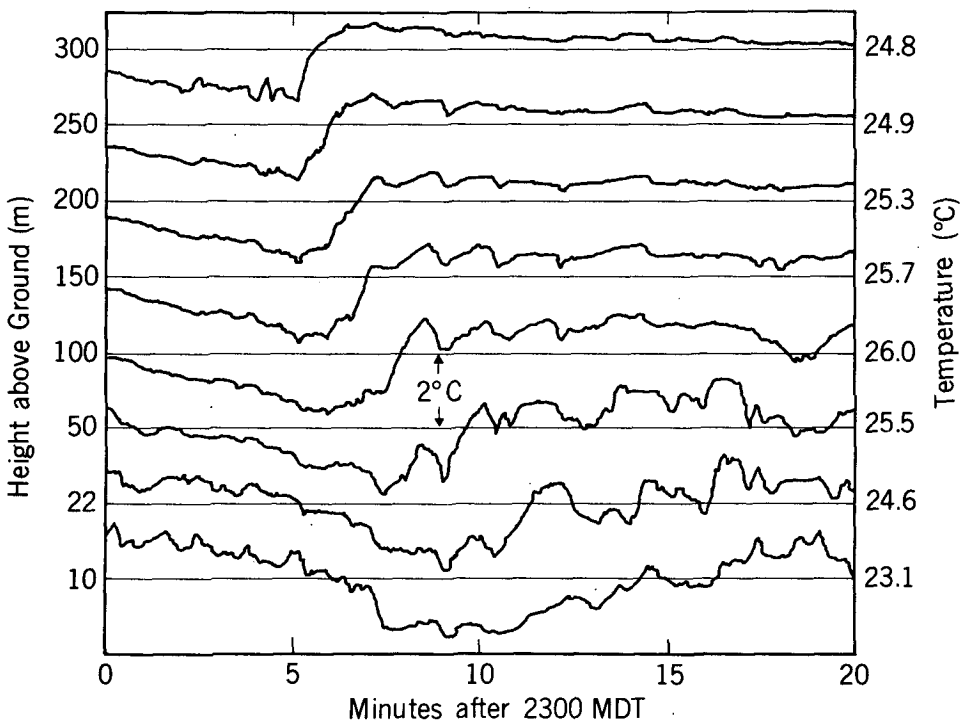

FIG. 8. Time series of tower-measured slow-response temperature at eight different heights for the period 2300–2320 MDT 1 July 1983, illustrating the lack of atmospheric stationarity during the measurement period. Acoustic sounder records showed evidence of breaking waves during roughly the same interval.

cumstances are necessary to evaluate the model properly.

Although this experiment demonstrated the applicability of lidar to measurements in moving reference frames, it also illustrated the problems that must be dealt with in analyzing and interpreting the data. Spatial averaging of fluctuations tends to attenuate the high-frequency region of the turbulence spectrum when the radial dimension of the scattering volume is long, as does the presence of noise caused by statistical variability in the lidar spectrum. This filtering effect should ultimately limit the use of lidar for examining turbulence effects on very large-diameter turbines. One way to extend the system's capability to simulate the larger turbines is to employ large diameter transceiver optics. Since the radial scattering volume dimension varies roughly as the inverse square of the optics diameter, as seen in Eq. (3), tripling the optics size reduces the radial measurement dimension by a factor of 10. Thus, use of 1-m diameter optics in this experiment would decrease the range resolution to approximately 6 m for the case of the largest turbine simulated, which would greatly enhance measurement quality at the higher frequencies through an increase of the cutoff frequency shown in Fig. 7 by an order of magnitude. It should be noted that 1 m optics are quite expensive; thus, increasing optics size may not be a practical solution.

The problem of measurement noise introduced by random fluctuations in the backscattered signal spectrum can be completely solved through improved signal processing. For these measurements we used a standard swept-filter spectrum analyzer for frequency analysis of the lidar signal. Since the time required to sweep through the Doppler spectrum and transfer the data to magnetic tape was 100 ms, only a single sample of the random spectrum was obtained per velocity sample. Simply improving the digitizing and data transfer efficiency, while still incorporating the spectrum anaylzer, could increase the spectrum-sampling rate to 10 per velocity sample. A much more significant reduction in measurement noise is obtainable by incorporating a more efficient spectral estimator, such as a filter bank or a surface acoustic wave (SAW) analyzer, so that many more independent representations of the signal spectrum are available per velocity sample. A commercially available SAW analyzer used in an airborne CW Doppler lidar (Vaughn and Woodfield, 1984) in the United Kingdom produces a spectral measurement every 50 μs; thus on the order of 1000 spectra could be averaged for each velocity estimate obtained at a 10 Hz rate. Averaging to this extent would reduce to a negligible level the measurement noise caused by statistical fluctuations.

Acknowledgments. The authors are thankful to J. R. Connell for suggesting and providing useful input throughout the course of this project, to F. F. Hall, Jr., who conceived the virtual turbine lidar measurement, to D. L. Davis and M. E. Jackson for their valuable assistance with the data analysis, and to T. R. Lawrence, M. J. Post and R. A. Richter for their help in obtaining the measurements. The contribution of W. D. Neff in interpretation of the acoustic sounder and tower sensor data is also gratefully acknowledged.

This work was partially funded under a grant from Battelle Pacific Northwest Laboratory, Richland, Washington.

REFERENCES

Connell, J. R., 1980: Turbulence spectrum observed by a fast-rotating turbine blade. Rep. PNL-3426, Battelle Pacific Northwest Laboratory, Richland, WA, 35 pp.

——, 1981: The spectrum of wind speed fluctuations encountered by a rotating blade of a wind energy conversion system: Observations and theory. Rep. PNL-4083, Battelle Pacific Northwest Laboratory, Richland, WA, 47 pp.

Dickson, L. D., 1969: Characteristics of a propagating Gaussian beam. *Appl. Opt.*, **9**, 1854–1861.

Frost, W., B. H. Long and R. E. Turner, 1978: Engineering handbook of the atmospheric environmental guidelines for use in wind turbine generator development. NASA Tech. Pap. 1359, 379 pp. [Available NTIS, U.S. Dept. of Commerce, Springfield, VA.]

Hardesty, R. M., 1986: Performance of a discrete spectral peak frequency estimator for Doppler wind velocity measurements. Accepted for publication *IEEE J. Geosci. Remote Sens.*, **GE24**, 777–783.

——, J. A. Korrell and F. F. Hall, Jr., 1981a: Lidar measurement of wind velocity turbulence encountered by a rotating wind turbine. U.S. Dept. of Energy Report DOE/RL/10236-81-1, 23 pp. [Available NTIS, U.S. Dept. of Commerce, Springfield, VA.]

——, R. J. Keeler, M. J. Post and R. A. Richter, 1981b: Characteristics of coherent lidar returns from calibration targets and aerosols. *Appl. Opt.*, **20**, 3763–3769.

——, T. R. Lawrence, R. A. Richter, M. J. Post, F. F. Hall, Jr. and R. M. Huffaker, 1983: Ground-based lidar measurement of tropospheric and stratospheric parameters. *Proc. SPIE*, **415**, 85–90.

Kaimal, J. C., and J. E. Gaynor, 1983: The Boulder Atmospheric Observatory. *J. Appl. Meteor.*, **22**, 863–880.

Kopp, F., R. L. Schwiesow and C. L. Werner, 1984: Remote measurements of boundary-layer wind profiles using a CW Doppler lidar. *J. Climate Appl. Meteor.*, **23**, 148–154.

Kristensen L., and S. Frandsen, 1982: Model for power spectra of the blade of a wind turbine measured from a moving frame of reference. *J. Wind Engin. Indus. Aerodyn.*, **10**, 249–262.

Lawrence, T. R., D. J. Wilson, C. E. Craven, I. P. Jones, R. M. Huffaker and J. A. L. Thomson, 1972: A laser velocimeter for remote sensing. *Rev. Sci. Instrum.*, **43**, 512–518.

Linscott, B. S., P. Perkins and J. Dennett, 1984: Large horizontal-axis wind turbines. NASA TM-83546, 73 pp. [Available NTIS, U.S. Dept. of Commerce, Springfield, VA.]

Schwiesow, R. L., R. E. Cupp, P. C. Sinclair and R. F. Abbey, Jr., 1981: Waterspout velocity measurements by airborne Doppler lidar. *J. Appl. Meteor.*, **20**, 342–360.

Vaughn, J. M., and A. A. Woodfield, 1984: Wind measurement with coherent laser radar at 10 μm. *Proc. ESA Workshop on Space Laser Applications and Technology*, Les Diablerets, Switzerland, 26–30 March, 231–237.

Verholek, M. G., 1978: Preliminary results of a field experiment to characterize wind flow through a vertical plane. Rep. PNL-2518, Battelle Pacific Northwest Laboratory, Richland, WA, 42 pp.